Published April 1, 1999

Energetic and Spatial Parameters for Gating of the Bacterial Large Conductance Mechanosensitive Channel, MscL

Sergei I. Sukharev,* Wade J. Sigurdson,‡ Ching Kung,§ and Frederick Sachs‡

From the *Department of Biology, University of Maryland, College Park, Maryland 20742; ‡Department of Physiology and Biophysical Sciences, State University of New York, Buffalo, New York 14214; and §Laboratory of Molecular Biology and Department of Genetics, University of Wisconsin, Madison, Wisconsin 53706

ABSTRACT MscL is multimeric protein that forms a large conductance mechanosensitive channel in the inner membrane of *Escherichia coli*. Since MscL is gated by tension transmitted through the lipid bilayer, we have been able to measure its gating parameters as a function of absolute tension. Using purified MscL reconstituted in liposomes, we recorded single channel currents and varied the pressure gradient (P) to vary the tension (T). The tension was calculated from P and the radius of curvature was obtained using video microscopy of the patch. The probability of being open (P_o) has a steep sigmoidal dependence on T, with a midpoint ($T_{1/2}$) of 11.8 dyn/cm. The maximal slope sensitivity of P_o/P_c was 0.63 dyn/cm per e-fold. Assuming a Boltzmann distribution, the energy difference between the closed and fully open states in the unstressed membrane was $\Delta E = 18.6\ k_B T$. If the mechanosensitivity arises from tension acting on a change of in-plane area (ΔA), the free energy, $T\Delta A$, would correspond to $\Delta A = 6.5\ nm^2$. MscL is not a binary channel, but has four conducting states and a closed state. Most transition rates are independent of tension, but the rate-limiting step to opening is the transition between the closed state and the lowest conductance substate. This transition thus involves the greatest ΔA. When summed over all transitions, the in-plane area change from closed to fully open was 6 nm^2, agreeing with the value obtained in the two-state analysis. Assuming a cylindrical channel, the dimensions of the (fully open) pore were comparable to ΔA. Thus, the tension dependence of channel gating is primarily one of increasing the external channel area to accommodate the pore of the smallest conducting state. The higher conducting states appear to involve conformational changes internal to the channel that don't involve changes in area.

KEY WORDS: mechanical • membrane • tension • stretch • kinetics

introduction

Mechanosensitive (MS)[1] channels or stretch-sensitive channels, discovered in chick skeletal muscle cells (Guharay and Sachs, 1984; Brehm et al., 1984) are likely candidates for the role of primary mechanoreceptors in unicellular and multicellular organisms. In the hair cells responsible for hearing and balance in vertebrates, MS channels are implicated in generation of primary potentials associated with the hair bundle displacement (Corey and Hudspeth, 1983). In nonsensory cells, MS channels have been shown to mediate mechanical stress-induced changes in membrane permeability to monovalent ions and Ca^{2+} (Sachs and Morris, 1998), potentially triggering cascades of second messenger signaling. In bacteria that live in a rapidly changing environment, mechanosensitive channels mediate permeation of small osmolytes from the cytoplasm through the periplasm to the extracellular space, potentially permitting a rapid regulation of turgor pressure (Saimi et al., 1993; Berrier et al., 1996; Blount et al., 1998).

MS channels are identified by their activities, not sequence similarities. Given the variety of observed ionic selectivities and gating properties, there is little evidence that they form a family by sequence similarity (Martinac, 1993). In eucaryotes, MS channel activity appears to require coupling to the cytoskeleton and/or the extracellular matrix, probably for the transmission of force (Sachs and Morris, 1998). In contrast, bacterial MscL is functional in lipid bilayers (Sukharev et al., 1994b).

Although some MS channels have been characterized biophysically, very little is known about their molecular structure. An extensive genetic dissection of the nematode *Caenorhabditis elegans* revealed ~20 genes involved in touch sensation (Driscoll and Chalfie, 1993; Tavernakis and Driscoll, 1998). Two of them are possible candidates for MS channel subunits, featuring close sequence similarity to the ENaC, the amiloride-sensitive Na^+ channel (Rossier et al., 1994). Other touch genes code for cytoskeletal or extracellular matrix components, presumably those elements necessary for the

S.I. Sukharev and W.J. Sigurdson contributed equally to this work and should be considered co-first authors.

Address correspondence to Wade J. Sigurdson, Ph.D., Dept. Physiology and Biophysics, 320 Cary Hall, SUNY at Buffalo, Buffalo, NY 14214. Fax: 716-829-2028; E-mail: wjs@buffalo.edu

[1]*Abbreviation used in this paper:* MS, mechanosensitive.

Published April 1, 1999

efficient transmission of forces to the channels. Unfortunately, there are only two descriptions of electrophysiological evidence for the mechanosensitive role of any of these genes (Awayda et al., 1995; Kizer et al., 1997).

As an alternative to the complexity of metazoa, MS channels in microorganisms are biochemically and genetically accessible (Martinac et al., 1992; Martinac, 1993; Sukharev et al., 1993, 1994a, 1997; Le Dain et al., 1998). Patch-clamp studies on native and reconstituted *Escherichia coli* membranes revealed three types of mechanosensitive channel (Msc) activities: MscL, MscS, and MscM (L, S, and M stand for large, small, and "mini" conductances, respectively; Berrier et al., 1996). Using a variety of chromatographic techniques followed by reconstitution and patch recording of channels in liposomes, MscL, the most conductive of MS channels in *E. coli* was identified as an ~17-kD protein, and the corresponding *mscL* gene was then cloned (Sukharev et al., 1994a).

Biochemical studies have shown that MscL resides in the inner membrane of *E. coli* (Blount et al., 1996a). Each MscL subunit is a 15-kD protein with two putative transmembrane domains and a high α-helical content (Arkin et al., 1998). Whereas the functional channel complex was proposed to be a homohexamer (Blount et al., 1996b), a recent crystallographic study indicates a pentameric structure for the closed state of the channel (Chang et al., 1998) MscL can be activated by 70–180-mmHg pressure gradients across patches of bacterial spheroplasts, and purified MscL channels reconstituted into phospholipid liposomes produced similar currents. This indicates that MscL can be gated directly by tension transmitted via the lipid bilayer alone. In vivo, the channel may be opened by osmotic gradients of 200–700 mOsm (Blount et al., 1998). MscL-like channels are found in several groups of eubacteria (Sukharev et al., 1997; Moe et al., 1998), and there is increasing evidence that MscL plays the role of a "safety valve" in prokaryotes, releasing small osmolytes, thereby reducing the turgor pressure and the chance of cell lysis.

In the present work, we quantitatively evaluate the energetic parameters for MscL gating in reconstituted liposomes using a similar approach as described by Opsahl and Webb (1994a). We used high-resolution video microscopy to measure the curvature of patches at different activating pressures, permitting us to calculate the absolute tension. Kinetic and thermodynamic analysis of the channel allows us to calculate the free energy differences between states and their tension dependence (Hamill and McBride, 1994). Close examination of the single channel conductance has identified at least four open conductance classes. Analysis of transition rate constants, using a simple linear Markov model, has permitted identification of the tension dependence of each rate constant between the closed and open conductance classes. This work represents the first calibration of a cloned, biological mechanosensitive ion channel.

methods

MscL Isolation and Reconstitution

The procedure for MscL purification using a 6His-tag has been described previously (Blount et al., 1996b; Sukharev et al., 1996). Briefly, a tag of six sequential histidines was added to the COOH terminus of MscL by a two-step PCR amplification and the extended gene was cloned into the pB10a vector (Sukharev et al., 1994a). The PB104 cells expressing MscL-6His were French-pressed and the total membrane fraction was isolated. The MscL-6His protein was extracted from membranes by solubilization in 3% β-octylglucoside and purified in one step using a Ni-NTA column (QIAGEN Inc.) as described (Sukharev et al., 1996). Azolectin (Soybean lecithin, type II; Sigma Chemical Co.), a lipid component of proteoliposomes, was partially purified from oxidized and lyso forms using chloroform/water separation. Briefly, 500 mg of azolectin beads were washed five times with 5–7 ml of acetone (electron microscopy grade), with gentle swirling after each change. After the last wash, the residual acetone was removed by vacuum (20 min) and the beads were dissolved in 5 ml of chloroform. The solution was placed in a thick-walled glass tube with a Teflon stopper, overlaid with 5 ml of water, and shaken vigorously. The cream-colored mixture was separated by 2 h centrifugation in a swinging-bucket rotor at 13,000 rpm at 15°C. The lower chloroform portion was retrieved by a long-needle glass syringe, placed in an airtight Teflon-capped vial, and could be stored at −20°C under nitrogen for ~1 mo.

MscL-6His was reconstituted into azolectin liposomes by dialyzing the β-octylglucoside-solubilized mixture of a protein-to-lipid ratio of 1:500 to 1:2,000 (Sukharev et al., 1994b). In special cases when we needed to record single MscL currents for kinetic analysis, the protein-to-lipid ratio was lowered to ~1:10,000. Proteoliposomes were subjected to a dehydration–rehydration cycle on glass slides (Sukharev et al., 1994b) and the resultant multilayer aggregates were placed in the recording buffer (see below) for 30–60 min before the patch-clamp experiment. Large, and apparently unilamellar, blisters formed on the surface of multilayer liposomes were examined as excised inside-out patches.

Channel Recording

Borosilicate glass pipettes with 1–2-μm bore diameter were used in all experiments. The pipette pulling protocol was adjusted to form long-tipped pipettes with an almost cylindrical, 10–20-μm–thick by 100-μm–long region before the tip. This narrow taper was useful for observation of liposome patches that tend to creep up the pipette under pressure gradients. To compensate for the headstage tilt and make the observed part of the pipette nearly parallel to the focal plane, pipette tips were bent as described previously (Sokabe et al., 1991). All recordings were performed in a symmetrical buffer containing 200 M KCl, 40 mM $MgCl_2$, and 10 mM HEPES, pH 7.2. Pressure gradients were delivered by either a pneumatic screw-driven syringe and monitored by an electronic pressure transducer or with a laboratory-built hydraulic pressure servo (Sachs, 1987; Sokabe et al., 1991). Patch currents were recorded at hyperpolarizing voltages (+20 mV in the pipette) using an Axopatch 200 (Axon Instruments) and stored on a PCM tape (48 kHz sampling rate; Instrutech Corp.). The second data channel on the recorder was allocated to recording pressure.

Published April 1, 1999

To determine P_o as a function of pressure, the data were analyzed using PCLAMP6. P_o was calculated as the mean patch conductance G_P divided by $n \cdot G_{MscL}$, where G_{MscL} is the maximal conductance of a single MscL channel (typically 3.5–3.7 nS) and n is the number of channels in the patch. n was estimated either by measuring the current at saturating pressures or, with less precision, by using the average number of channels per patch in a given proteoliposome preparation determined in separate experiments. When n was >10, the patch conductance, G_P, was corrected to account for the series pipette resistance ($R_S \cong 1.5$–2 MΩ) by the equation, $G_P = I/(V - IR_S)$, where V and I are the transmembrane voltage and current, respectively. We made >200 attempts to record complete activation curves for MscL in different settings and, of these, fifteen were considered extensive enough to warrant analysis. They compose the data presented below. Experiments were usually terminated by lysis of the patch.

Kinetic Analysis

For the multistate analysis, we used the QuB program suite (www.qub.buffalo.edu). To determine the rate constants between states, the digitized data was first idealized using SKM, a Hidden Markov algorithm (Feng et al., 1996; Qin et al., 1996). The "events list" outputs from SKM were then grouped as a global collection of data sets over defined tension. This tension series was fit to a kinetic model using MIL, a maximum likelihood interval analysis program that permits data to be fit across independent variables and corrects for missed events (Qin et al., 1995). Since we determined there were five states (four subconducting and one shut state), the number of possible kinetic connections was extremely large (728 models). We were able to exhaustively search all models and connectivities using the program MSEARCH, which employs MIL to rank all models, based on the likelihood calculated for each model. For all nonlooping models, the linear sequential model gave the greatest likelihood, and therefore was used for the analysis: C1–S2–S3–S4–O5, where C, S, and O refer to the closed, subconductance, and open states, respectively.

To determine how the single channel MscL conductance depends on the bath conductivity, we recorded currents from reconstituted channels in baths containing 10 mM HEPES, pH 7.2, and 40 mM $MgCl_2$, with KCl concentrations varied between 0.1 and 2 M. The specific conductivity of each buffer was measured directly using a YSI 34 Conductance Meter equipped with a dip-type glass cell with platinized platinum-iridium electrodes (1.0 cm cell constant; Yellow Springs Instrument Co.). Single-channel currents were recorded at +20 mV (pipette voltage), and the unitary current of the fully open state was determined using FETCHAN's 'Measure' function (PCLAMP suite; Axon Instruments).

Patch Imaging and Determination of Curvature

Patches were imaged using an inverted microscope (Axiovert; Carl Zeiss, Inc.) equipped for Differential Interference Contrast with a CCD camera as initially described by Sokabe et al. (1991). The digitized images were analyzed with an algorithm written in JAVA by Akinlaja (1997) that solved for the radius of curvature.

To avoid confusion within equations, T will reference tension, while temperature T will only appear as a term with the Boltzmann constant; i.e., k_BT.

results

Previous patch-clamp experiments revealed that activation of MscL requires pressures close to the lytic tension of the unmodified bilayer (Martinac, 1993; Sachs and Morris, 1998). This proximity made it difficult to obtain many data sets with saturating responses. Typically, activation in spheroplast patches required 70–200 mmHg, while liposome patches needed 40–150 mmHg. Patches formed with large-diameter pipettes activated at lower pressures, suggesting that the actual parameter that drives MscL gating is tension, not pressure. Prolonged exposure of patches to high pressures often caused lysis. This imposed strict requirements on the stability of the bilayer in which the channels were reconstituted. A partially purified crude phospholipid fraction from soybean (azolectin) gave us acceptable stability and reproducibility of results. Under a small pressure gradient, liposome patches, lacking cellular components, are spherical caps and are large enough to be viewed by conventional optical microscopy. Experiments were considered successful if we were able to obtain enough points to fit the partial activation curve with $P_o > 0.3$ with images of the patch of sufficient quality to calculate the curvature.

Analysis of the Data as a Two-State System

As the data below will show, MscL is not a binary channel, but has multiple conducting states. However, some of the essential features of the gating process can be

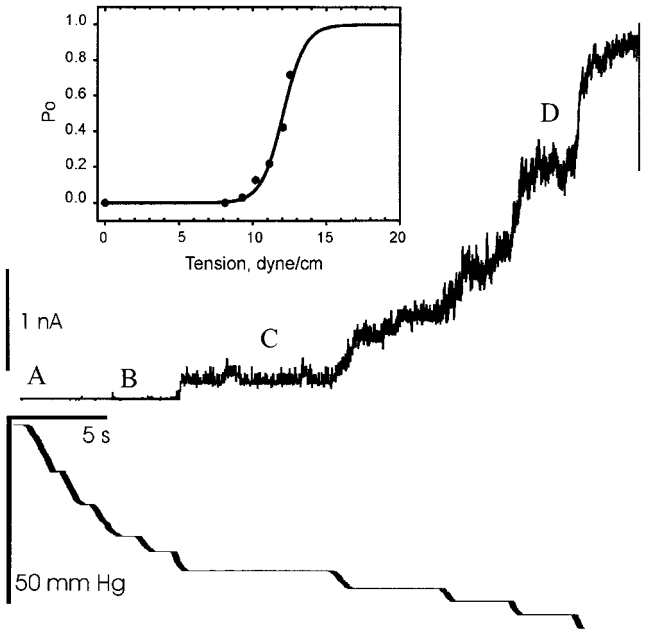

FIGURE 1. The current (top) activated in a multichannel patch by increasing suction (bottom). The highest suction reached in this experiment was 54 mmHg, at which point the patch ruptured (vertical current spike at the right margin). The patch conductance derived from this trace was corrected for the series pipette resistance R_s and the MscL open probability (see METHODS) was then plotted against pressure (inset). The labels on the current trace correspond to the images shown in Fig. 2.

Published April 1, 1999

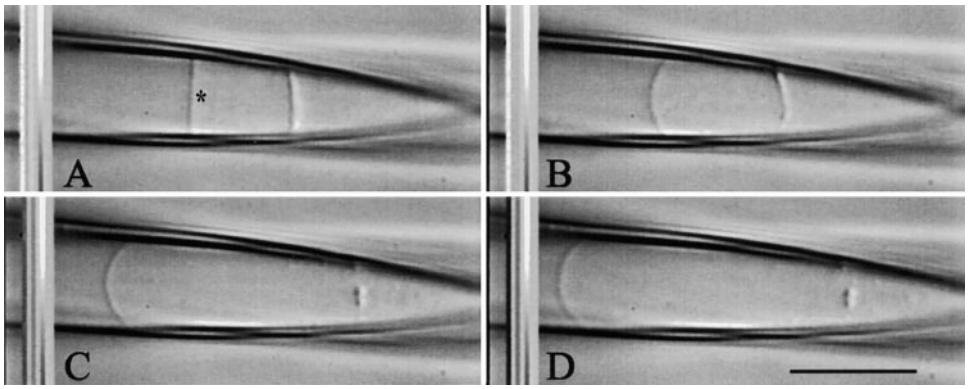

FIGURE 2. The geometry of the patch at pressure gradients of 0 (A), 20 (B), 42 (C), and 52 (D) mmHg, imaged simultaneously with the current recording shown in Fig. 1. (A) At zero pressure, the patch membrane (*) was practically flat. As the pressure gradient increased, the radius of curvature decreased and the geometry became stable beyond 40 mmHg. A and B show a fragment of membrane located toward the tip, but not bearing tension as shown by the opposite curvature. The vertical striped bars located on the left side of the images are analogue data records multiplexed onto the video signal (see Zhang et al., 1997). Scale bar, 10 μm.

gained from considering the simpler two-state model, a model that would correspond to the data viewed at low bandwidth. This analysis is based on setting a threshold for being open at half the fully open state amplitude. Previous data indicated that mean current MscL pressure–activation curves can be well fit with single component Boltzmann distribution. Our initial experiments were designed to determine the midpoint ($T_{1/2}$) and the maximum slope of this distribution, the two key parameters of the dose–response curve. Only one parameter, $T_{1/2}$, actually requires the measurement of patch curvature. An accurate measure of the slope can be obtained from $P_o(P)$ curves measured "blindly" (i.e., without geometric measurements), provided that the radius of curvature is independent of the pressure (see below).

Fig. 1 shows a typical trace from a patch containing ~100 MscL channels in response to a stepwise increase of pressure gradient P (bottom). The MscL current activates at ~40 mmHg and increases with P in a nonlinear manner. Note that in the beginning of the trace the variance of the current (amplitude of fluctuations around the mean level) increases with each step, reaches a maximum, and finally decreases during the last pressure step before the patch ruptures. The maximum of the current variance indicates the point at which $P_o = 0.5$; thus the half-maximal pressure $P_{1/2}$ is between 48 and 52 mmHg for this particular recording (Fig. 1, D). The R_s-corrected dose–response curve derived from this trace is shown in Fig. 1, inset.

Fig. 2 shows the geometry of the same patch at pressure gradients of 0, 20, 44, and 52 mmHg. In the absence of suction, the patch is essentially flat, subjected to the "resting" tension arising from membrane adhesion to the glass surface (Fig. 2 A; Opsahl and Webb, 1994b). At low suction, the patch appears as a spherical cap, with a progressively increasing curvature (Fig. 2 B). At higher suction, the curvature saturates because the membrane is nearly inextensible (see calculation below). At higher suctions, the patch may creep up the pipette (Fig. 2 D). This creep does not affect the geom-

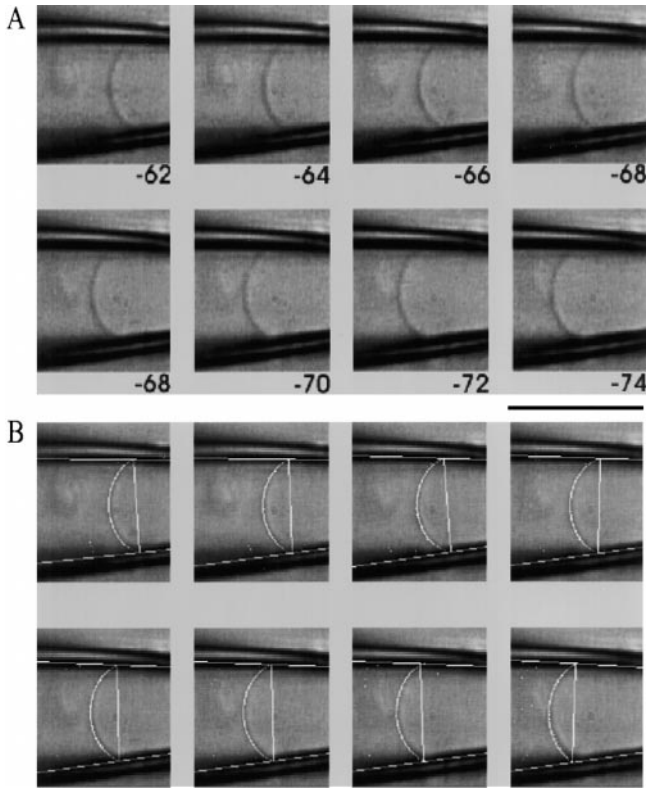

FIGURE 3. Curve fitting images of the patch. (A) Increasing pipette suction produces only small changes in the radius of curvature while the patch membrane slowly creeps upward into the pipette. The amount of pipette suction (mmHg) is indicated in each frame. (B) The location of the pipette walls and the patch membrane, as determined by the image-fitting program, are superimposed onto the images. Scale bar, 9 μm.

Published April 1, 1999

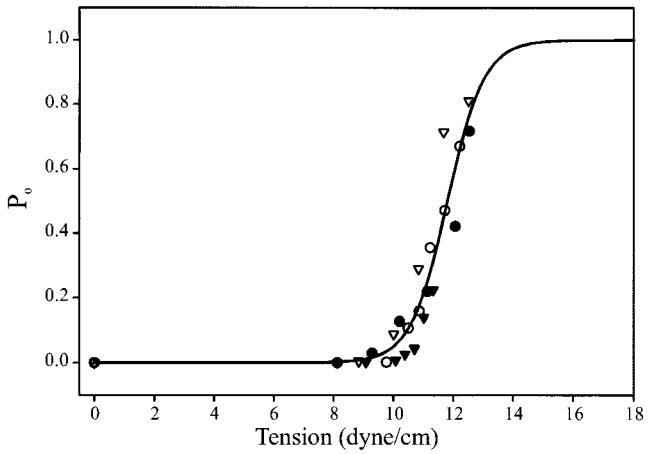

FIGURE 4. Partial dose–response (open probability–tension) curves measured for four independent patches. The curvature of each individual patch was fit as shown in Fig. 3. Using the patch radius and the pressure, $P_o(P)$ curves were transformed into $P_o(T)$ curves according to Laplace's law. The simultaneous fit of all these curves with a Boltzmann distribution gave a midpoint $T_{1/2}$ of 11.8 dyn/cm and a slope of 0.61 dyn/cm per e-fold (P_o/P_c ratio).

etry significantly as long as the pipette taper is small. As seen in Fig. 1, MscL channels are only active for $P > 40$ mmHg. This is the range of pressures where the patch curvature reaches saturation so that one measurement of the curvature was adequate to calculate the tension for all pressures where MscL is active. The procedure of fitting the patch curvature is depicted in Fig. 3.

We have been able to obtain partial activation curves from four independent patches, in which we were also able to measure the radius of curvature, *r*. The membrane tension was calculated for every pressure according to Laplace's law, $T = p \times r/2$, and the P_o data were plotted against *T* as shown in Fig. 4. The patches were fit as a group to a single Boltzmann function with $T_{1/2} = 11.8 \pm 0.8$ dyn/cm and a maximal slope of 0.61 ± 0.17 dyn/cm per e-fold change of P_o/P_c.

More precise and statistically reliable estimates for the slope of $P_o(T)$ curves were obtained from the analysis of additional $P_o(P)$ experiments done without measurement of the patch curvature, but aligned to $T_{1/2} = 11.81$ dyn/cm. Given that the patch curvature does not change significantly in the range of pressures where MscL is active (compare Fig. 3), the two scales, *T* and *P*, are equivalent with $T_{1/2} = r \times P_{1/2}/2$. Measuring $P_o(P)$ curves alone is much easier than the simultaneous geometric measurement. 11 complete $P_o(P)$ curves obtained from three independent MscL preparations were fit independently with a Boltzmann curve. $P_{1/2}$ was determined individually for each curve, and then rescaled to the same midpoint, $T_{1/2} = 11.81$ dyn/cm. As shown in Fig. 5, the curves display a remarkable consistency and, when fitted together, indicate the slope factor of 0.63 ± 0.08 dyn/cm.

If interpreted in the framework of a two-state Boltzmann model with the change of in-plane area being the dominant energy term, $T\Delta A$, we have:

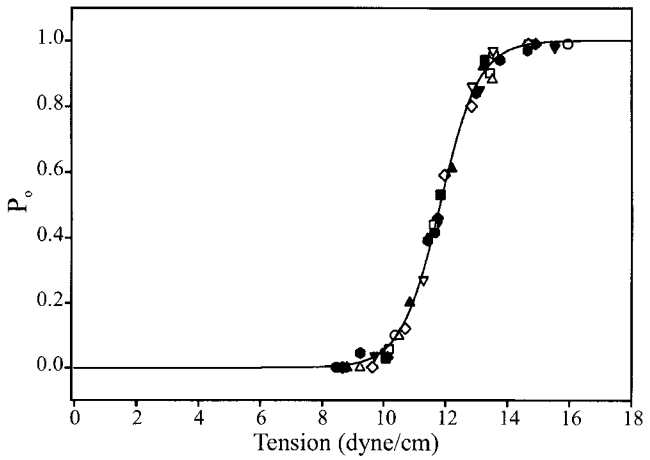

FIGURE 5. A statistical evaluation of the slope for dose–response curves. 11 $P_o(P)$ curves taken without patch imaging were converted to $P_o(T)$ dependencies by rescaling to the same midpoint $T_{1/2}$ of 11.81 dyn/cm and fit to the Boltzmann two-state model (Sachs and Morris, 1998). The mean slope factor for this set of curves is 0.63 dyn/cm (per e-fold change of P_o/P_c).

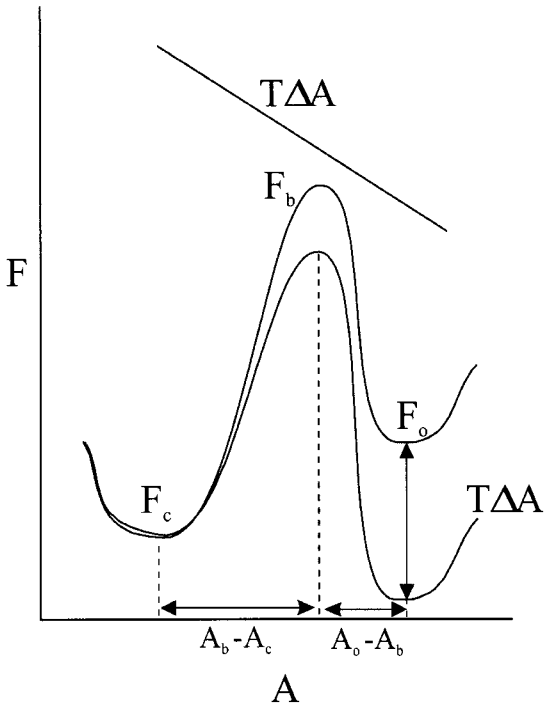

FIGURE 6. An energy diagram of the two-state channel model as a function of the in-plane area A of the channel. F represents the Helmholtz free energies of the closed (c) and open (o) states and the barrier peak (b). $T\Delta A$ is the change in energy between the closed and open channels at tension *T*. Relative to the model in the text, $a = (A_c - A_b)/k_BT$, where the *A* is the area of the channel in the relevant parts of the reaction path, $\Delta A = A_o - A_c$. The tension does the work of $T\Delta A$ when the channel (in either state) changes area by ΔA (upper linear curve).

$$P_o = 1/[1 + \exp(\Delta E - T\Delta A)/k_B T]. \quad (1)$$

Fitting to Eq. 1 gave $\Delta E = 18.61\ k_B T$ (46.3 kJ/mol) for the free energy of the closed-to-open transition in the absence of stress, and $\Delta A = 6.52$ nm^2 for the in-plane change in area between closed and open ($k_B T$ is Boltzmann's constant × the absolute temperature = 4.04×10^{-14} erg at room temperature).

In a more specific representation of the two-state model, we can write the forward and backward rates as:

$$k_{on} = k_0 \exp(-a \times T) \text{ and} \quad (2)$$

$$k_{off} = k_0 \exp(-b \times T), \quad (3)$$

where k_0 is a scaling factor incorporating $T_{1/2}$ and a and b are functions of the energies between the energy wells and the top of the barrier separating the states (Fig. 6). For example, $a = \Delta A_c / k_B T$, where ΔA_c is the increase of in-plane area between the closed state and the top of the energy barrier. The units of a are inverse tension (cm^2/erg = cm/dyne). Since the probability of being open, $P_o = k_{12}/(k_{12} + k_{21})$, the Boltzmann equation assumes the form $P_o/P_c = \exp[(a - b)\ T]$.

Fig. 7 represents typical single-channel traces illustrating the MscL kinetics at different tensions (A) and semi-logarithmic tension dependencies of rate constants for opening and closing transitions (k_{on} and k_{off}) derived from these traces according to a two-state model (B). The dependence of $\ln(P_o/P_c)$ for the same patch illustrates the rate at which the equilibrium occupancies of open and closed states change with tension. The tension dependence of the rate of opening (k_{on}) is about equal to that of $\ln(P_o/P_c)$. The tension dependence of the rate of closing is four times less. This suggests that the shortening of the closed state makes a larger contribution to the change of P_o than the lengthening of the open state. From the tension dependence of the rate constants, we estimate that $A_c - A_b$ is ≈ 4.42 nm^2 (equivalent to a disk of radius 1.19 nm) and $A_o - A_b \approx 1.37$ nm^2, (equivalent to a disk of radius 0.7 nm). The total area change, based on transition rates be-

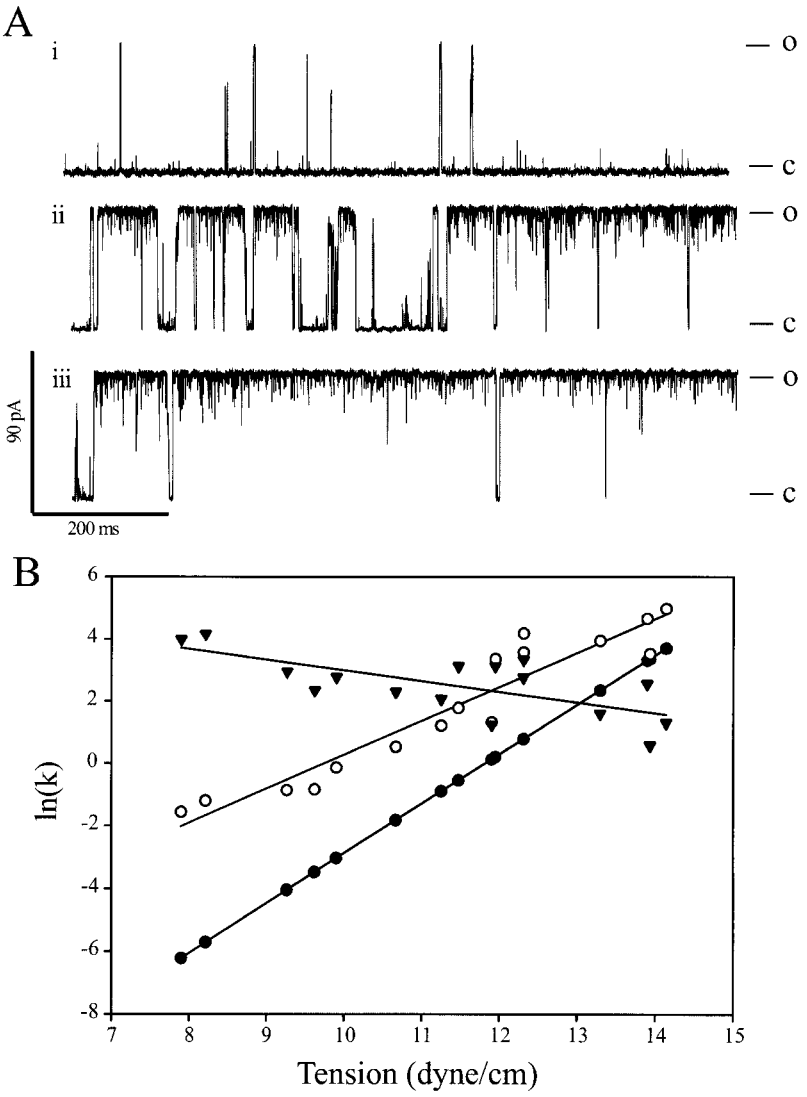

FIGURE 7. MscL kinetics at different tensions, analyzed with a two-state model. (A) Representative traces obtained on one patch containing a single MscL at three different membrane tensions. Tension and P_o for A, i–iii, were 9.6, 12.3, and 14.1 dyn/cm and 0.028, 0.689, and 0.976, respectively. Data were decimated fivefold and low-pass filtered at 2 kHz. (B) Logarithms of rate constants for opening (k_{on}, ○) and closing (k_{off}, ▼) as a function of tension. The $\ln(P_o/P_c)$ for all data sets (●) is shown for comparison. The slopes, m, and correlation coefficients are: $\ln(P_o/P_c)$ m = 1.59, r^2 = 0.999; $\ln(k_{on})$ m = 1.093, r^2 = 0.90; $\ln(k_{off})$ m = −0.34, r^2 = 0.48.

Published April 1, 1999

tween closed and open, is therefore 5.8 nm^2, as compared with 6.5 nm^2 calculated from P_o. As shown below, the channel is not a two-state system and therefore a discrepancy may be expected.

The Multi-State Analysis

The above analysis was done as though the channel were a two-state system with rate constants calculated from dwell times generated according to a half-amplitude detection criterion (Sachs et al., 1982; Colquhoun and Sigworth, 1983). Closer examination of the data, however, shows multiple conducting states (Fig. 8). The conductances illustrated in Fig. 8 are shown in Table I, along with estimates of the pore radius calculated assuming a cylindrical pore 4.2-nm long (Cruickshank et al., 1997).

While the minimal reaction scheme for so many states would normally be difficult to determine reliably, exploration of the likelihood of all possible interconnections (Feng et al., 1996; see METHODS) indicated that the simple sequential model (shown below) was the best fit for all nonlooping models (Table II).

The rate constants for all patches are plotted as a function of tension and are shown in Fig. 9. The straight lines are nonlinear regressions to a simple exponential of $k = k_0 \exp(\alpha T)$ with the residuals weighted by the inverse of the variance provided by MIL. The parameters of the regression are shown in Table III. Most striking is that only k_{12} has a significant positive slope; all other rates are insensitive or have negative slopes. In the simple free energy model presented above, the tension sensitivity α can be identified with $\Delta A / k_B T$. One needs to bear in mind, however, that the sign of α will change with the direction of the reaction. A transition from a well to a barrier will produce

t a b l e i

Conductance of the Different States of MscL Obtained Using the Program SKM

State	Conductance	SD	r_{pore}
	ns	*ns*	*nm*
C1	0	—	0
S2	1.03	0.3	0.8
S3	2.53	0.14	1.4
S4	3.23	0.168	1.7
O5	3.57	0.23	1.8

C, closed; S, substate; and O, fully open state. The mean conductance and SD are shown. The states are labeled according to Fig. 8. The radius refers to that calculated assuming the channel to be cylindrical and 4 nm in length.

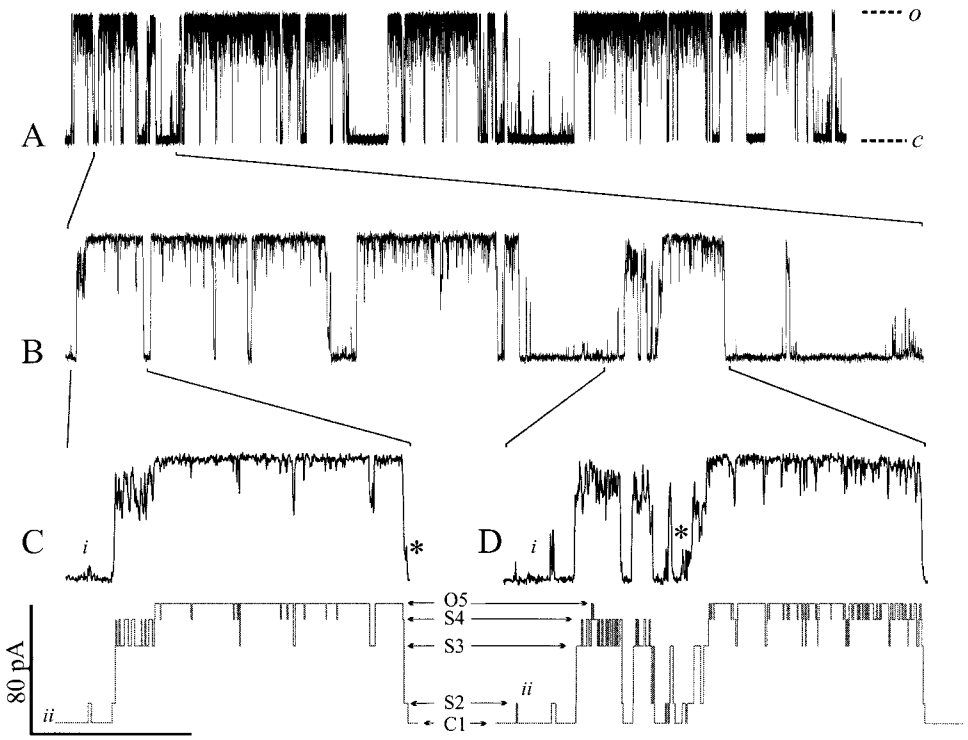

FIGURE 8. A plot of the single channel currents from MscL at different time scales illustrating multiple conducting states. The state amplitudes are noted as C1, S2, S3, S4, and O5 for the closed, subconductance 1–3, and open states, respectively. (A) Low-time resolution showing average MscL gating activity (P_o = 0.67). O and C represent the fully open and closed states, respectively. Time scale bar, 800 ms. (B) An expanded segment of A demonstrates the multiple conductance levels typical of this channel (time scale bar, 80 ms). Two expanded segments of B are shown in C_i and D_i, showing in more detail the four open conductance levels and MscL opening and closing via substates, some of which have been marked with *. Time scale, 15 and 20 ms, respectively. Below the current traces are idealizations (C_{ii} and D_{ii}) produced by SKM for segments C_i and D_i. These show the relative amplitudes of each of the four conductance classes. (Solutions: symmetrical 200 mM KCl 40 mM $MgCl_2$, 10 mM HEPES, pH 7.2; membrane potential, 20mV; membrane tension, 12.3 dyn/cm).

Published April 1, 1999

t a b l e ii

Log Likelihood Values for the Five Best Nonlooping Models Ranked in Decreasing Order as Determined by the Program MSEARCH (see METHODS)

	Data sets log (likelihood)	
Scheme No. and ranking	1	2
1	33273.94	11335.55
2	32702.6	11310.97
3	32306.31	11242.07
4	31774.98	11220.71
5a	31708.48	—
5b	—	11196.84

All five-state Markov models (768 in total) were tested on two data sets (1 and 2) obtained at different membrane tensions (P_O = 0.67 and 0.98, respectively). Of all schemes, Scheme I (a linear scheme with sequentially increasing substate conductances) was the model with the greatest likelihood and was chosen for subsequent estimation of the rate constants. In the reaction schemes, C denotes closed; O, open; and S, subconducting states. The state numbering is arbitrary. Blank entries represent lack of convergence of the fit, which occurs with models possessing a flat likelihood space.

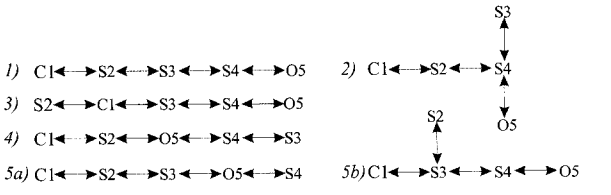

(SCHEME I)

the opposite change in area than moving from the barrier to the same well.

To summarize the kinetics contained in Fig. 9 and Table III, we have plotted in Fig. 10 the energy profiles of the states and the changes of in-plane area. Fig. 10 shows again that the rate limiting step to opening channel is k_{12}, for which the energy barrier is $\sim$38 k_BT. At zero tension, the energy difference between the closed and any of the conducting states is $>$18 k_BT, accounting for the fact that the channel is almost never open at rest. All states of conductance $>$S1 have about the same energy and are insensitive to tension. Applying tension lowers the energy of all the conducting states (energy wells) and barriers equally. The dimensional changes of the channel are shown in Fig. 10, bottom, where we plotted a running sum of the area changes accompanying each transition. As expected from the tension sensitivity, the area changes associated with changing states are small except for the transition from closed to S1. The total change of in-plane area between the closed and open states is 5–6 nm^2, as estimated from the two-state analysis.

How well does the above analysis fit reasonable physical models of the channel? There are two types of information we can use to estimate the physical structure: the pore diameter and the channel protein properties. The channel conductance gives information about the aqueous pore, and the protein properties give estimates of the wall thickness. We measured the MscL full conductance state as a function of bath conductivity. As shown in Fig. 11, the fully open single channel conductance was linear with the conductivity up to 2 M KCl. The absence of saturation and the lack of anion/cation selectivity is consistent with the representation of the open MscL as a wide aqueous pore. The conductance data were fit with the Hille equation describing conductance of a cylindrical pore (Hille, 1992), and the results are shown in Table IV. The first column corresponds to the assumed length of the channel. The calculated cross-sectional area suggests that the open MscL channel has a diameter of 2.7–3.6 nm, which is in good agreement with the data reported recently by Cruickshank et al. (1997). The value for in-plane area expansion during gating estimated from the two-state analysis (above), ΔA = 6.5 nm^2, is in the same range estimated for the pore cross-section, $5.8 > A > 9.7$ nm^2 (see Table IV).

Having an estimate of the open channel pore diameter, we now need to estimate the wall thickness to obtain the outer diameter where the bilayer tension is applied. The channel is a pentamer, with each monomer containing two helical transmembrane segments (Blount et al., 1996b; Arkin et al., 1998; Cheng et al., 1999). Given that the fully open channel will have a pore diameter of $\sim$4 nm, there are barely enough α helices to coat an aqueous pore of the estimated diameter if the helices make a close-contact circle around the pore. Using 1 nm as an estimate for helix diameter, the outer diameter of the open channel will be $\sim$6 nm. Alternatively, adding the change in radius of $\sim$0.5 nm (calculated from the change in area seen by gating) to the crystal radius of the closed channel (2.5 nm; Cheng et al., 1999) predicts an outer diameter of open channel of 5.5 nm.

The structure of the lower conductance states, however, is less well constrained since the in-plane area changes associated with gating do not match the changes in conductance. If internal pore reorganization is involved in setting the conductance of the closed and substates, we would predict each substate to exhibit a distinct dependency on the ionic composition of the bath.

d i s c u s s i o n

MscL, the first mechanosensitive channel for which some structural characteristics are available, now has quantitative parameters that can be used to judge the effects of mutagenesis and pharmacology. The ability to use a fluid bilayer for reconstitution eliminated the

Published April 1, 1999

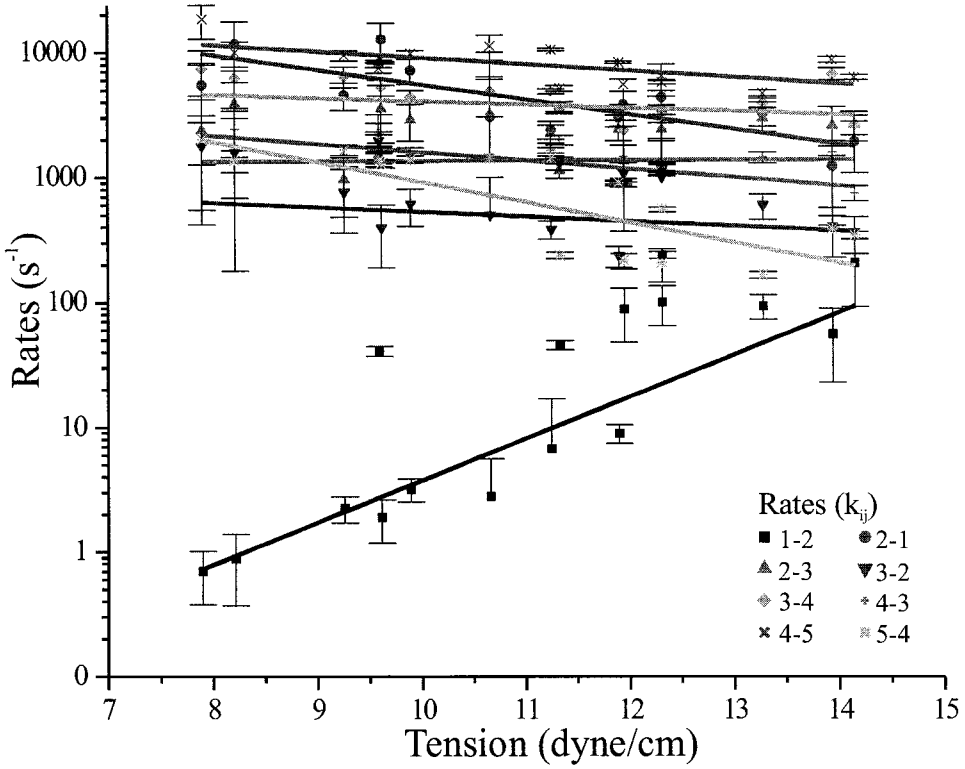

FIGURE 9. The rate constants vs. tension for the linear sequential model (inset, the respective rate constant symbols). The rate constants were obtained using the program MIL and the regression lines were calculated as fits to single exponential functions of tension with weights determined by the estimated variance of the parameters produced by MIL. The rate-limiting step in opening is k_{12}, corresponding to the rate of going from closed to the smallest conductance substate. The plot includes data from five different patches.

need to deal with the complex mechanics of heterogeneous biological membranes. The low bending moment of bilayers assured the membranes were spherical so that the pressure gradient could be simply translated into tension according to Laplace's law. Since bilayers have substantial resistance to area changes, there was little change in curvature once the membrane assumed a spherical shape. The image-fitting algorithm used to determine patch curvature was limited by the optical resolution of the microscope (~0.35 μm), such that changes in the radius of curvature could not be reliably detected at the higher pressures. The expected changes can be predicted from an equation describing the stretch of an elastic membrane attached to the pipette walls (Sokabe et al., 1993):

$$P = (4K_A/a)\,(T/K_A)^{3/2}/(1 + T/K_A), \qquad (4)$$

where K_A is the area elastic constant of the membrane and a is the radius of the pipette where it meets the patch. Using Laplace's law, we can then solve for the radius of curvature r as a function of pressure. Inserting a few constants makes the behavior clear. Consider a soft membrane with $K_A = 100$ dyn/cm and a patch with $a = 2$ μm. For $P = 50$ mmHg (1 mmHg = 1.33×10^3 dyn/cm^2), $r = 3.33$ μm and for 100 mmHg, $r = 2.76$ μm, a change of 20%. For a stiffer membrane with $K_A = 500$ dyn/cm, the same pressures give $r = 5.44$ and 4.38 μm, a change of 24%. Thus, in this pressure range, the tension is nearly proportional to the pressure.

The set of data in Fig. 4 shows that the tension to activate MscL is near the lytic strength of the bilayer. The $P_o(T)$ curves have a midpoint of 11.8 dyn/cm, which exceeds the critical tension for mechanical breakdown of many phospholipid bilayers (Bloom et al., 1991). This is also close to the lytic tension for bacterial mem-

TABLE III

Calculated Transition Rate Constants for the Linear Reaction Scheme, Scheme I of Table II

k_{ij}	k_0 (s^{-1})	SD	α	SD	$\Delta S/k_B$	$\Delta\Delta S/k_B$
k_{12}	0.0016	0.0052	0.78	0.29	36.4	—
k_{21}	85163	54297	−0.27	0.06	18.6	17.8
k_{23}	1280	1293	0.005	0.09	22.8	—
k_{32}	1247	2995	−0.09	0.20	22.8	0.0
k_{34}	7491	5439	−0.06	0.06	21.0	—
k_{43}	7338	5813	−0.15	0.07	21.0	0.0
k_{45}	29851	19962	−0.12	0.06	19.6	—
k_{54}	36857	74350	−0.37	0.17	19.4	0.2

Rates were derived by optimizing across data sets obtained at different tensions on a given patch. To combine the data from different patches, each rate constant was subjected to an exponential regression against tension using data from all patches, as shown in Fig. 9. The rate constants are of the form: $k_{ij} = k_0\exp(\alpha \cdot T/k_BT)$, where k_0 is the tension independent component and α is the tension sensitivity. SD, the calculated standard deviation of the regression parameters (assuming a Gaussian distribution of errors). The true errors are clearly not Gaussian since there is zero probability of k_0 actually being negative, but they are included as rough guidelines. Much of the scatter arises from differences between patches, perhaps caused by differences in the resting tension of the membrane. The activation entropies, ΔS, and the differences in ΔS between states, $\Delta\Delta S$ were calculated from k_0 according to the Eyring model (see text).

Published April 1, 1999

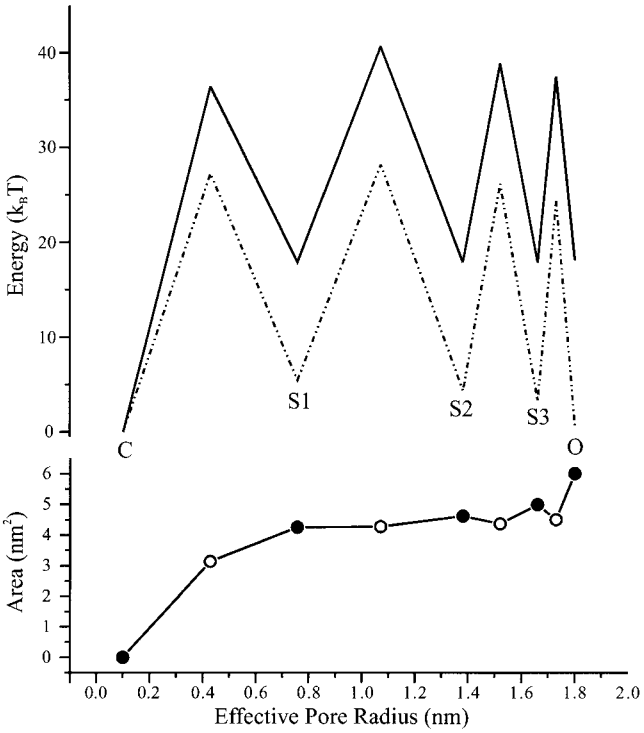

FIGURE 10. The energy profiles and area changes of MscL states. (Top) The energy of the states at rest (solid line) and at a tension of 11.8 dyn/cm, midway in the activation curve (dotted line). The energies have been referenced to the closed state. The resting state energies were calculated from the preexponential term of the rate constants assuming the Eyring form of a rate: $k = k_BT/h \exp(-\Delta S/k_B)$, where h is Planck's constant and ΔS is the entropy of the reaction. The energies while under tension were calculated from $k = k_BT/h \exp(T\Delta A/k_BT - \Delta S/k_B)$. The effective pore radii were calculated from our conductance data assuming a cylindrical pore 4.2-nm long and arbitrarily giving the closed channel a radius of 0.1 nm (see DISCUSSION). (Bottom) The integrated change of in-plane area as the channel moves from closed to open (calculated from $\alpha = T\Delta A$ in Table III).

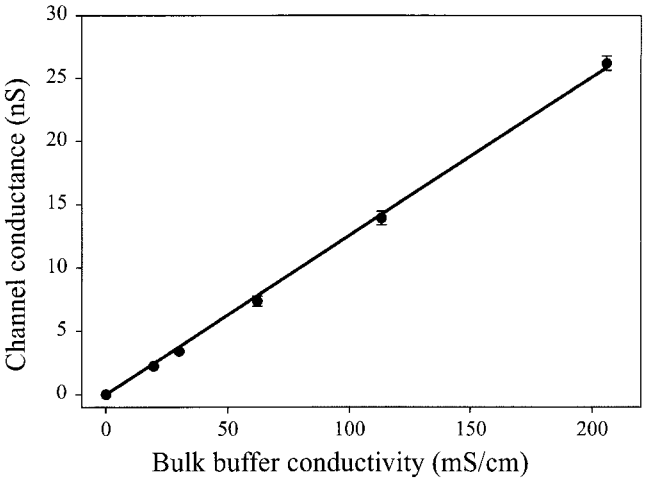

FIGURE 11. The dependence of single-channel conductance on the conductivity of the bathing solution. Hille's equation, $G_{ch} = \rho\pi a^2/(l + \pi a/2)$, linking the channel conductance to the length of the pore (l), its radius (a), and specific electrolyte conductance (ρ) was used to fit the curve. The corresponding pore diameter (d) and cross-sectional area (s), were estimated from the slope of the curve are shown in Table IV.

branes as suggested by frequent lysis of spheroplast patches at tensions that activate MscL. This proximity is consistent with the proposed "safety valve" function for MscL as a pore that can dissipate osmotic gradients when the membrane stability is in danger. In a cell of 1-μm diameter, the osmotic gradient required to create a tension of 12 dyn/cm is 20 mOsm, corresponding to a pressure of 360 mmHg. Soil bacteria may experience much larger osmotic stresses during rainfall. Knockouts of MscL have not shown osmotic fragility, however, and this is probably caused by the presence of other more sensitive mechanical channels, including MscS and MscM (Martinac, 1993; Berrier et al., 1996). MscL may become active and release larger osmolytes only at extremely strong downshocks, >200 mOsm, as indicated by osmotically-induced ATP efflux (Sukharev, unpublished observations).

The nonsaturable character of MscL conductance (Fig. 11) and the absence of anion/cation selectivity (Sukharev et al., 1993b) strongly suggest a large water-filled pore. The specific conductivity of electrolyte inside the pore would then be similar to its bulk value and, therefore, the "macroscopic" equations deriving the channel conductance from its geometry and conductivity are reasonable (Hille, 1992). The length of the channel pore was estimated to be ≈4 nm from sieving data (Cruickshank et al., 1997).

The energetics of MscL gating suggests that this channel undergoes large changes in dimensions, accounting for its steep dose–response curve. MS channel gating is, by definition, a function of force (Corey and Hudspeth, 1983; Sachs and Lecar, 1991; Sachs and Morris, 1998). The simplest model for planar mechanical free energy is based on the notion that if the open channel occupies a larger area than the closed channel, then tension favors opening. This model was used in the energy diagram of Fig. 6, although it should be pointed

TABLE IV

Estimated Geometrical Parameters for the MscL Main State Pore from its Conductance in Solutions of Different Conductivity

Pore length	Pore cross-section	Pore diameter
nm	*nm^2*	*nm*
5	9.72	3.52
4	8.24	3.24
3	6.60	2.90
2	5.80	2.72

The dimensions were calculated assuming the pore to be cylindrical and fitting to the data in Figure 11.

Published April 1, 1999

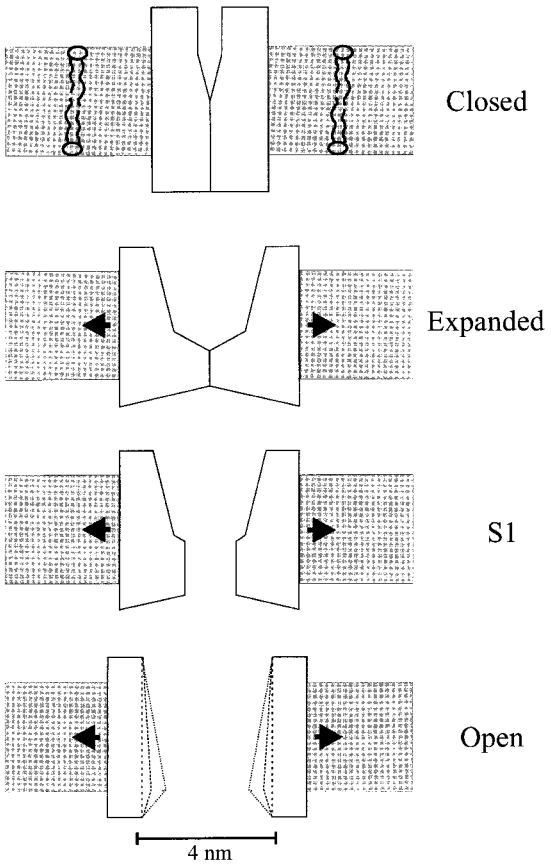

FIGURE 12. Cartoon of a cross-sectional view of the channel as it opens suggested by the calculated energy landscape. The channel progresses from the closed conformation (Closed), experiences an increase in membrane tension (Expanded), gates to the first substate (S1), and, through a series of internally reorganized substates, to the fully open state (Open). Open shows the pore diameters for the subconductance states as dashed lines. The channel outer diameter increases primarily in the closed-to-S1 transition. The gating process is likely preceded by an elastic deformation of the entire channel complex, noted as expanded. The opening rate is limited by the first gating transition to S1. The subsequent transitions are largely tension independent and lead to the open state. The drawing of the open state is to scale with the outer diameter of the fully open state ~6 nm with a pore diameter of 3.6 nm, corresponding to a ring of five to six alpha helices surrounding the pore.

out that while the figure is drawn with finite widths for the wells and barriers, the mathematics assumes the barrier is a delta function and the wells are boxes.

The dose–response curves in Fig. 5 were well fit by Eq. 1 with parameters $\Delta E = 18.6\ k_B T$ (46.3 kJ/mol) and $\Delta A = 6.5\ \text{nm}^2$. Both numbers are large at the molecular scale and their combination makes the MscL dose–response curve steep. The large value of ΔE predicts that the open probability at low tension ($T < 1$ dyn/cm) would be $\sim 10^{-8}$. Indeed, with no mechanical stimulus, the impedance of a patch with >200 MscLs is >1 GΩ—closed channels are not leaky and have almost no spontaneous activity. If MscL opened spontaneously, it would dissipate the proton gradient within ~1 μs and disrupt cell energetics.

Using the slope of the tension–sensitivity curve, we can compare MscL gating energetics with other channels. Alamethicin (Opsahl and Webb, 1994a) and the mechanically sensitive cation-selective channel found in chick skeletal muscle (Sokabe et al., 1991) have similar sensitivities on the order of 3–8 dyn/cm per e-fold change in P_o. The yeast (Gustin, 1991) and bacterial MS channels described here have much steeper slope sensitivities (0.05 and 0.63, respectively), indicative of large area changes between closed and open states. The midpoints of the activation curves were quite different, however, with the yeast MS channel reaching half max with only 0.7 dyn/cm tension (Gustin, 1991) as compared with MscL, which required 11.8 dyn/cm. The setpoints and sensitivities of the MS channels so far examined appeared to be tuned to respond to membrane tension in very different ways, perhaps reflecting the different physiological roles.

The similarity between the size of the MscL pore and the change of in-plane area ΔA_{oc} is striking, and the basic relationship is maintained in the multistate analysis, where the C–S1, instead of C–O, is rate limiting. These dimensional changes strongly suggest that the opening of the pore constitutes the major part of the entire protein complex expansion. When the rate constants of Table I are taken explicitly in terms of an Eyring model, differences in k_0s reflect differences in the entropy of activation. In turn, the entropy is a measure of deformability, with narrow energy wells representing stiff conformations and wide energy wells representing soft conformations (Sachs and Lecar, 1991). The rate constant k_{12} has the largest entropy change of all the rates, suggesting that the closed state is quite flexible relative to the excited state (the peak of the barrier between 1 and 2). If we examine the change of stiffness between states by calculating the entropy differences, $\Delta\Delta S$, the only significant change of stiffness is between the closed state and S1. Thus, the closed state seems to be the only one sufficiently soft to allow the available tension to do significant work on the channel.

Do these results agree with structural information? Each MscL subunit (15 kD, 136 amino acids) spans the membrane twice with both termini intracellular. The two transmembrane domains are most likely α helical and oriented normal to the membrane as judged by circular dichroism (Arkin et al., 1998). Although initial cross-linking experiments had suggested that the functional MscL complex is a homohexamer (Blount et al., 1996b; Sukharev et al., 1997), more recent and extensive cross-linking studies and the crystal structure of the closed channel indicate a pentameric stoichiometry (Cheng et al., 1999). Images of negatively stained two-dimensional crystals of tag-purified MscLs revealed

Published April 1, 1999

hexagonal lattices of doughnut-shaped particles (Le Dain et al., 1998) that were recognized as hexamers. The resolution of unsymmetrized projection maps achieved in this work does, however, seem to be insufficient to draw an unambiguous conclusion on the number of subunits in the complex. As discussed by Cruickshank et al. (1997), twelve transmembrane helices would be just sufficient to line a pore ≈4 nm in diameter. The 30 amino acid periplasmic loop might be a part of the pore lining of the open channel, but is clearly within the cytoplasm in the closed channel (Cheng et al., 1998).

In examining the energetic model as illustrated in Fig. 10, the question arises as to why the increase in conductance from S1 to O5 (presumably an increase in cross-sectional area of the channel) is not correlated with a significant increase in the tension sensitivity—we know that the conductance, and presumably pore diameter, is increasing. There are two types of explanations: (a) the in-plane area really doesn't increase very much, or (b) the free energy available from tension described as $T\Delta A$ is incomplete. Explanations for a could involve increases in conductance from shortening the pore, rather than increasing the cross-section. Alternatively, there may be more complicated conformational changes to the pore interior that affect ion transport. Explanations for b might involve components of free energy such as the line tension, a term proportional to the perimeter of the channel that has the opposite sign to $T\Delta A$. Line tension plays a role in the stability of pores in lipid bilayers (Zhelev and Needham, 1993). Or, we could have stress-induced changes in channel (water?) entropy that would affect the free energy (Sachs and Lecar, 1991). Currently, we cannot separate these various components, but the relative simplicity of internal pore reorganization as a method to alter conductance (Fig. 12) has appeal from studies on mechanically insensitive channels.

To account for the similarity of ΔA for the rate-limiting step and the pore diameter, the closed conformation would have to exclude most of the water from its interior (∼15–30 nm^3), presumably becoming some sort of compact, ion-impermeable, bundle. If the helices remain normal to the membrane, the pore cannot be closed by steric interactions unless the channel forms a close packed trimer. If the helices twist about the pore axis, the effects of pore diameter are minor as long as the pore diameter is comparable to the membrane thickness. If the helices rotate axially, forcing hydrophobic faces toward the pore, the channel might close using ordered water as the "gate" (Sachs and Feng, 1993), but this seems unlikely given the large diameter of the structure. If the channel closed by using the extracellular domain as a gate, then the agreement of the pore cross-section with the ΔA_{co} must be assumed coincidental.

Regardless of details, there are large dimensional changes involved in opening MscL; changes much larger than proposed for other channels. Our analysis has focussed on state models because of the clear finite residence times in the different conducting states. However, the large and rapid dimensional changes associated with gating probably also involve inertial components that affect the current rise times. Since the propagation velocity of shear waves in lipids are on the order of 10 nm/ms (Debregeas et al., 1998), there may be useful physical details in the form of the transition currents, particularly those between C and S1.

Recently, Gu et al. (1998) proposed an electromechanical model of MscL gating that involves the NH_2-terminal domains as gates, pivoting under stress from a position parallel to the membrane to one normal to the plasmalemma. The model attempts to calculate the electrostatic force between specific charged residues located on the NH_2- and COOH-terminal domains and those on the membrane-spanning helices. Membrane tension causes the extracellular end of the helices to tilt inward, changing the distances between the charges, lowering the force that causes the NH_2-terminal domains to swing to a normal position with respect to the bilayer. However, the balance of electrostatic forces between charged residues was calculated without accounting for electrolyte screening, which dictates that in 0.2 M salt there will be almost no interaction between two unitary charges positioned 1-nm apart. Our experimental data show there is no significant change in the gating pattern in the range of salt concentration between 0.05 and 1 M. This practically excludes the role of long-range electrostatic interactions in MscL gating. MscL is also weakly voltage dependent, which is contrary to the model where an external field must strongly influence the distribution between open and closed states.

The Gu et al. (1998) model also imposes strict constraints on the length and charge of the NH_2-terminal domain. This region must be about the pore radius in length, and six of them must occlude the pore completely, as we know that closed MscL is absolutely nonleaky. This is difficult to satisfy and also contradicts the work of Blount et al. (1996c) and Hase et al. (1997), whose data show that the removal of 3, substitution of 8, or addition of 20 new residues to this domain doesn't significantly change the channel gating.

The model assumes the closed channel is already in a fully patent configuration; i.e. the 4-nm pore is present through all of the open and most of the closed states. Although the model predicts a small increase in area during gating, the ∼6-nm^2 area increase we calculate (which accounts for the steepness of the dose–response curve) is much larger than predicted. Even if the channel operates through a combination of area changes that pull the gates to a lower energy state followed by

Published April 1, 1999

the NH_2-terminal swinging gates, our evidence for large area changes does not seem compatible with their model. However, the subconductance states could result from individual terminal domains partially interfering with permeation.

Considerations of Our Results in the Context of the Recent Three-Dimensional Structure of MscL

As this paper was in the process of review, Dr. Doug Rees (California Institute of Technology, Pasadena, CA) kindly shared with us a preprint of the full x-ray structure of an MscL homolog (Chang et al., 1998) and we felt that it was useful to make a first-order comparison with our results. The structure looks like two barrels in series—a wide one in the transmembrane portion and a narrow one in the intracellular compartment. The channel is a pentamer with each subunit having two alpha helical transmembrane domains tilted at ~28° and an intracellular helical domain. The intracellular domains form a 3.5-nm continuation of the pore. The result is a channel ~8.5 nm in length with a diameter that varies from ~1.8 to 0.2 nm, the latter representing the gate in the closed channel. This putative gating region consists of a ring of hydrophobic residues located near the intracellular depth of the bilayer. The outer diameter of the transmembrane portion, where tension is applied, is ~5 nm.

The most striking contrast with our results (and other published results) comes from the expected channel conductance. Knowing the open channel conductance, and modeling it as a cylindrical pore, we can calculate that a channel 4 nm in length must have a diameter >3 nm to have a conductance of ~3 nS (Table IV). If the pore were opened to its maximal 1.8-nm diameter along its entire 8.5-nm length, the predicted conductance would be ~0.5 nS instead of the calculated 3.2 nS. If, upon opening, the intracellular pore domain were assumed to unfold completely, the transmembrane length would be ~5 nm and the conductance 0.85 nS. Since the simple cylindrical model (Hille, 1992) assumes no interaction of ions with the channel, the ions are point charges, and there are no image forces, the conductance estimate should be a maximum. Furthermore, since the channel is nonselective between anions and cations and its conductance is exactly proportional to the solution conductance up to 2 M KCl, we cannot invoke local fixed charges as concentrators of ions to increase conductance. It would appear that opening of the channel must involve major alterations in conformation that both shorten and widen the channel. The constraints are clear if we suppose tension causes the channel to splay into a cone with the narrow end of the pore remaining at the observed 1.8-nm diameter (presumably with the narrow end extracellular). As with a cylindrical pore, the conductance of a tapered pore consists of two convergence resistances and the pore resistance given by $R_{\text{pore}} = \rho\, l/\pi\, r_1 \times r_2$, where the r is the radii at each end, ρ is the solution resistivity, and l is the pore length. If the intracellular portion of the channel were folded out of the way against the bilayer so the pore was only 4-nm long, we would still have to expand the internal diameter to 100 nm to get the observed 3-nS conductance. Constraining even one end of the channel to 1.8-nm diameter strongly limits the possible pore conductance. However, it is perhaps not surprising that the pore dimensions of the closed channel differ greatly from the dimensions predicted for the open pore.

Concerning the structural origin of the mechanical sensitivity, the tension sensitivity can be explained by a modest increase in the outer diameter of the transmembrane domain from ~5.0 to 5.5 nm. If each of the 10 transmembrane helices were 12–13 nm in diameter and arranged in a close-packed ring normal to the membrane, the outer diameter would be 5–6 nm, in the range necessary to account for the mechanical sensitivity. If tension untwists the transmembrane helices to form a set of barrel staves perpendicular to the membrane, the cytoplasmic domains may peel away, shortening the length of the pore. The substates we observed may reflect such movements of the cytoplasmic helices. These domains, which are outside the bilayer, should not be strongly driven by membrane tension, making them compatible with the lack of tension sensitivity of the higher conductance substates.

There are methodological questions to be resolved between the crystallography and the electrophysiology. The crystals were formed in solutions at pH 3.7 and were stabilized with glutaraldehyde as well as heavy metal compounds, including Gd^{+3}, which is a known blocker of the channel. These conditions may create structures different from the native state and physiological tests need to be made on channels treated this way. Nonetheless, it is a thrill to have a real structure to examine and we eagerly await a structure of the open channel.

In summary, we have performed the first calibration of a biological mechanosensitive ion channel. These measurements place strong constraints on kinetic and structural models of MscL and related channels.

We thank the United States Army Research Office, National Aeronautics and Space Administration, and the National Institutes of Health for grant support.

Original version received 17 June 1998 and accepted version received 3 February 1999.

references

Akinlaja, J. 1997. Electromechanical rupture of cell-attached patches. Physics. Thesis/Dissertation. SUNY at Buffalo, Buffalo, NY. 1–56.

Arkin, I.T., S. Sukharev, P. Blount, C. Kung, and A.T. Brunger. 1998. Helicity, membrane incorporation, orientation and thermal stability of the large conductance mechano-sensitive ion channel from *E. coli*. *Biochim. Biophys. Acta*. 1369:131–140.

Awayda, M.S., I.I. Ismailov, B.K. Berdiev, and D.J. Benos. 1995. A cloned renal epithelial Na^+ channel protein displays stretch activation in planar lipid bilayers. *Am. J. Physiol.* 268:C1450–C1459.

Berrier, C., M. Besnard, B. Ajouz, A. Coulombe, and A. Ghazi. 1996. Multiple mechanosensitive ion channels from *Escherichia coli*, activated at different thresholds of applied pressure. *J. Membr. Biol.* 151:175–187.

Bloom, M., E. Evans, and O.G. Mouritsen. 1991. Physical properties of the fluid lipid-bilayer component of cell membranes: a perspective. *Q. Rev. Biophys.* 24:293–397.

Blount, P., M.J. Schroeder, and C. Kung. 1998. Mutations in a bacterial mechanosensitive channel change the cellular response to osmotic stress. *J. Biol. Chem.* 272:32150–32157.

Blount, P., S. Sukharev, M. Schroeder, S. Nagle, and C. Kung. 1996a. Mutations that change gating properties of a mechanosensitive channel in *E. coli*. *Biophys. J.* 70:A366. (Abstr.)

Blount, P., S.I. Sukharev, P.C. Moe, S.K. Nagle, and C. Kung. 1996b. Towards an understanding of the structural and functional properties of MscL, a mechanosensitive channel in bacteria. *Biol Cell.* 87:1–8.

Blount, P., S.I. Sukharev, P.C. Moe, M.J. Schroeder, R.H. Guy, and C. Kung. 1996c. Membrane topology and multimeric structure of a mechanosensitive channel protein of *Escherichia coli*. *EMBO (Eur. Mol. Biol. Organ.) J.* 15:4798–4805.

Brehm, P., R. Kullberg, and F. Moody-Corbett. 1984. Properties of non-junctional acetylcholine receptor channels on innervated muscle of *Xenopus Laevis*. *J. Physiol. (Lond.)*. 350:631–648.

Chang, G., R.H. Spencer, A.T. Lee, M.T. Barclay, and D.C. Rees. 1998. Structure of the MscL homolog from *Mycobacterium tuberculosis*: a gated mechanosensitive ion channel. *Science*. 282:2220–2226.

Colquhoun, D., and F.J. Sigworth. 1983. Fitting and statistical analysis of single-channel records. *In* Single-Channel Recording. B. Sakmann and E. Neher, editors. Plenum Publishing Corp., New York. 191.

Corey, D.P., and A.J. Hudspeth. 1983. Kinetics of the receptor current in bullfrog saccular hair cells. *J. Neurosci.* 3:962–976.

Cruickshank, C.C., R.F. Minchin, A.C. Le Dain, and B. Martinac. 1997. Estimation of the pore size of the large-conductance mechanosensitive ion channel of *Escherichia coli*. *Biophys. J.* 73:1925–1931.

Debregeas, D., P.G. de Gennes, and F. Brochard-Wyart. 1998. The life and death of "bare" viscous bubbles. *Science*. 279:1704–1707.

Driscoll, M., and M. Chalfie. 1993. The mec-4 gene is a member of a family of *Caenorhabditis elegans* genes that can mutate to induce neuronal degeneration. *Nature*. 349:588–593.

Feng, Q., A. Auerbach, and F. Sachs. 1996. Estimating single channel kinetic parameters from idealized patch-clamp data containing missed events. *Biophys. J.* 70:264–280.

Gu, L., W. Liu, and B. Martinac. 1998. Electromechanical coupling model of gating the large mechanosensitive ion channel (MscL) of *Escherichia coli* by mechanical force. *Biophys J.* 74:2889–2902.

Guharay, F., and F. Sachs. 1984. Stretch-activated single ion channel currents in tissue-cultured embryonic chick skeletal muscle. *J. Physiol. (Lond.)*. 352:685–701.

Gustin, M.C. 1991. Single-channel mechanosensitive currents. *Science*. 253:800.

Hamill, O.P., and D.W. McBride, Jr. 1994. The cloning of a mechano-gated membrane ion channel. *Trends Neurosci.* 17:439–443.

Hase, C.C., A.C. Le Dain, and B. Martinac. 1997. Molecular dissection of the large mechanosensitive ion channel (MscL) of *E. coli*: mutants with altered channel gating and pressure sensitivity. *J. Membr. Biol.* 157:17–25.

Hille, B. 1992. Ionic Channels of Excitable Membranes. Sinauer Associates Inc., Sunderland, MA. 185–188.

Kizer, N., X.L. Guo, and K. Hruska. 1997. Reconstitution of stretch-activated cation channels by expression of the alpha-subunit of the epithelial sodium channel cloned from osteoblasts. *Proc. Natl. Acad. Sci. USA*. 94:1013–1018.

Le Dain, A.C., N. Saint, A. Kloda, A. Ghazi, and B. Martinac. 1998. Mechanosensitive ion channels of the archaeon *Haloferax volcanii*. *J. Biol. Chem.* 273:12116–12119.

Martinac, B. 1993. Mechanosensitive ion channels: biophysics and physiology. *In* Thermodynamics of Cell Surface Receptors. M. Jackson, editor. CRC Press, Boca Raton, FL. 327–351.

Martinac, B., A.H. Delcour, M. Buechner, J. Adler, and C. Kung. 1992. Mechanosensitive ion channels in bacteria. *In* Comparative Aspects of Mechanoreceptors. F. Ito, editor. Springer-Verlag, Berlin. 3–18.

Moe, P.C., P. Blount, and C. Kung. 1998. Functional and structural conservation in the mechanosensitive channel MscL implicates elements crucial for mechanosensation. *Mol. Microbiol.* 28:583.

Opsahl, L.R., and W.W. Webb. 1994a. Lipid-glass adhesion in gigasealed patch-clamped membranes. *Biophys. J.* 66:75–79.

Opsahl, L.R., and W.W. Webb. 1994b. Transduction of membrane tension by the ion channel alamethicin. *Biophys. J.* 66:71–74.

Qin, F., A. Auerbach, and F. Sachs. 1995. Maximum likelihood estimation of kinetic parameters for single channels from dwell-time sequences. *Biophys. J.* 68:A79. (Abstr.)

Qin, F., A. Auerbach, and F. Sachs. 1996. Idealization of single channel currents using the segmental K-means method. *Biophys. J.* 70:A227. (Abstr.)

Rossier, B.C., C.M. Canessa, L. Schild, and J.D. Horisberger. 1994. Epithelial sodium channels. *Curr. Opin. Nephrol. Hypertens.* 3:487–496.

Sachs, F. 1987. Baroreceptor mechanisms at the cellular level. *Fed. Proc.* 46:12–16.

Sachs, F., and Q. Feng. 1993. Gated, ion-selective channels observed without membranes: novel properties of the gigaseal. *Biophys. J.* 65:1101–1107.

Sachs, F., and H. Lecar. 1991. Stochastic models for mechanical transduction. *Biophys. J.* 59:1143–1145.

Sachs, F., and C. Morris. 1998. Mechanosensitive ion channels in non specialized cells. *In* Reviews of Physiology and Biochemistry and Pharmacology. M.P. Blaustein, R. Greger, H. Grunicke, R. Jahn, L.M. Mendell, A. Miyajima, D. Pette, G. Schultz, and M. Schweiger, editors. Springer-Verlag, Berlin. 1–78.

Sachs, F., J. Neil, and N. Barkakati. 1982. The automated analysis of data from single ionic channels. *Pflügers Arch.* 395:331–340.

Saimi, Y., B. Martinac, A.H. Delcour, P.V. Minorsky, M.C. Gustin, M.R. Culbertson, J. Adler, and C. Kung. 1993. Patch clamp studies of microbial ion channels. *Methods Enzymol.* 207:681–691.

Sokabe, M., F. Sachs, and Z. Jing. 1991. Quantitative video microscopy of patch clamped membranes—stress, strain, capacitance and stretch channel activation. *Biophys. J.* 59:722–728.

Sokabe, M., W.S. Sigurdson, and F. Sachs. 1993. Effect of excision and cytochalasin on the viscoelastic properties of patch clamped membranes in heart and skeletal muscle. *Biophys. J.* 61:A513. (Abstr.)

Sukharev, S., P. Blount, M. Schroeder, and C. Kung. 1996. Multi-

meric structure of bacterial mechanosensitive channel MscL. *Biophys. J.* 70:A366. (Abstr.)

Sukharev, S.I., P. Blount, B. Martinac, F.R. Blattner, and C. Kung. 1994a. A large conductance mechanosensitive channel in *E. coli* encoded by MscL alone. *Nature*. 368:265–268.

Sukharev, S.I., P. Blount, B. Martinac, and C. Kung. 1997. Mechanosensitive channels of *Escherichia coli*: the MscL gene, protein and activities. *Annu. Rev. Physiol.* 59:633–657.

Sukharev, S.I., B. Martinac, P. Blount, and C. Kung. 1994b. Functional reconstitution as an assay for biochemical isolation of channel proteins: application to the molecular identification of a bacterial mechanosensitive channel. *Methods: A Companion to Methods in Enzymology.* 6:51–59.

Sukharev, S.I., B. Martinac, and C. Kung. 1993. Reconstitution of two distinct types of mechanosensitive channels from the *E. Coli* envelope. *Biophys. J.* 61:A93. (Abstr.)

Tavernakis, N., and M. Driscoll. 1998. Molecular modeling of mechanotransduction in the nematode *Caenorhabditis elegans*. *Annu. Rev. Physiol.* 59:659–689.

Zhang, B., W.J. Sigurdson, and F. Sachs. 1997. Storing analog data in a video record. *J. Neurosci. Methods.* 76:151–155.

Zhelev, D.V., and D. Needham. 1993. Tension stabilized pores in giant vesicles: determination of pore size and pore line tension. *Biochim. Biophys. Acta*. 1147:89–104.